




Intriguing behavior of $\text{UCo}_{1-x}\text{Rh}_x\text{Ge}$ ferromagnets in magnetic field along the b axis

Jiří Pospíšil ^{1,2,*}, Yoshinori Haga,¹ Atsushi Miyake,³ Shinsaku Kambe,¹ Yo Tokunaga,¹ Masashi Tokunaga,³ Etsuji Yamamoto,¹ Petr Proschek ², Jiří Volný,² and Vladimír Sechovský²

¹Advanced Science Research Center, Japan Atomic Energy Agency, Tokai, Ibaraki 319-1195, Japan

²Charles University, Faculty of Mathematics and Physics, Department of Condensed Matter Physics, Ke Karlovu 5, 121 16 Prague 2, Czech Republic

³The Institute for Solid State Physics, University of Tokyo, Kashiwa, Chiba 277-8581, Japan

 (Received 29 April 2020; revised 26 June 2020; accepted 29 June 2020; published 28 July 2020)

Single crystals of solid solutions of ferromagnetic superconductors UCoGe and URhGe were investigated by magnetization and specific-heat measurements. These compounds behave as anisotropic ferromagnets with the easy-magnetization direction along the orthorhombic c axis. The maximum Curie temperature $T_C = 20$ K has been observed in $\text{UCo}_{1-x}\text{Rh}_x\text{Ge}$ for $x = 0.4$. The main interest of the study was the intriguing behavior in magnetic fields applied along the b axis. The temperature dependence of the b -axis magnetic susceptibility exhibits a maximum at a characteristic temperature T_{max} . For low Rh concentrations ($x < 0.4$) $T_{\text{max}} > T_C$ and the magnetic entropy S_{mag} at T_C is very low, whereas $T_{\text{max}} = T_C$ and the S_{mag} at T_C is much higher for $x \geq 0.4$. A metamagneticlike anomaly in magnetization is observed in all compounds, at a critical field which appears on a similar energy scale with the value of the corresponding T_{max} . The character of three paramagnetic regimes which can be distinguished in the T - x and H - x phase diagrams, normal, correlated, and field polarized, is discussed in relation to the field-induced reentrant superconductivity in the parent compounds.

DOI: [10.1103/PhysRevB.102.024442](https://doi.org/10.1103/PhysRevB.102.024442)

I. INTRODUCTION

The $5f$ -electron ferromagnets URhGe [1] and UCoGe [2] occupy a prominent position in condensed-matter physics owing to the unconventional superconductivity in the ferromagnetically ordered phase. Both compounds crystallize in the same orthorhombic TiNiSi -type structure and are isoelectronic. They also exhibit the same type of strong magnetocrystalline anisotropy, which is the essence for the anisotropic features of the superconducting state. The easy magnetization direction is the c axis, while the a axis is the hardest magnetization direction. Metamagneticlike phenomena occur when fields are applied along the b axis, and significantly affect superconductivity [3–5]. Comparative research of these two materials, and the solid solution series between them, can deepen the understanding of unconventional superconductivity.

A jump in the magnetization of URhGe for $H||b$ is observed at a characteristic field of ≈ 12.5 T (in the literature marked as H_R [6,7]). This anomaly reflects a first-order transition involving the reorientation of the magnetic moment from the c to the b axis [8,9] leading to a loss of ferromagnetic ordering. This process induces strong ferromagnetic spin fluctuations and affects superconductivity. The field induced reentrant superconducting phase has the maximum superconducting temperature T_{SC} in the vicinity of H_R [4]. The b -axis magnetization of UCoGe at 1.5 K shows an upturn in the magnetization isotherm at ≈ 47.5 T [3] (in the literature marked as H_m [3]) which is more than three times higher on an energy scale than the field of ~ 15 T where the superconductivity in

UCoGe becomes reinforced [3,10]. Moreover, in contrast to URhGe , the superconductivity is suppressed by a magnetic field applied along b very shallowly creating a broad, so far experimentally unbounded, superconducting dome with upper critical field H^b_{c2} apparently exceeding 20 T [11,12].

The field of the broad metamagneticlike anomaly on the low-temperature magnetization isotherm in UCoGe is comparable in energy scale to T_{max} , where a broad maximum in the temperature dependence of magnetic susceptibility, $\chi(T)$ [13], appears. Such a maximum was observed on the $\chi_b(T)$ curve for the $H||b$ axis of UCoGe at 37.5 K [3] which is far above $T_C = 2.5$ K. On the other hand, a sharp peak at $T_{\text{max}} = T_C = 9.5$ K [3,14,15] was found for URhGe .

Superconductivity in URhGe [8,15] and UCoGe [12,16,17] has been intensively studied. In contrast, much less attention has been paid to the magnetization behavior in the normal state, particularly to the paramagnetic range in the neighborhood of the ferromagnetic domes in their complex H - T phase diagrams. The remarkably different magnetization behavior of UCoGe and URhGe stimulates a study of the evolution of the characteristic magnetization behavior over the entire pseudoternary $\text{UCo}_{1-x}\text{Rh}_x\text{Ge}$ system. Such a study, which has been done on polycrystals [18], revealed a nonmonotonous concentration dependence of Curie temperature. The intrinsic anisotropic magnetization features, especially these in fields applied along the b axis, could not be explored because the measured magnetization bears only information on the average of the magnetization components along the three crystallographic axes.

It is worth mentioning that the recently discovered superconductivity in UTe_2 [19,20] exhibits similarities to the behavior of ferromagnetic superconductors despite it having a

*Corresponding author: jiri.pospisil@mff.cuni.cz

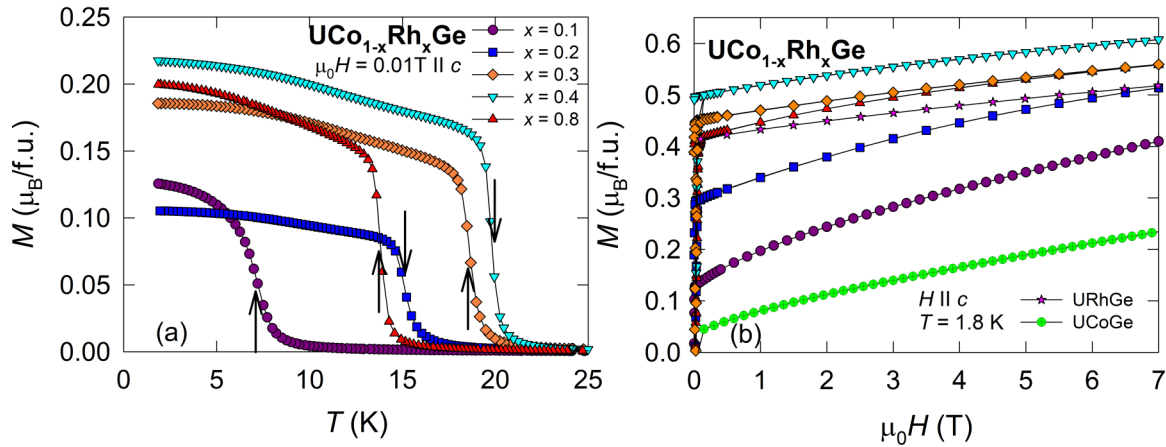


FIG. 1. (a) Thermomagnetic curves and (b) magnetization isotherms of $\text{UCo}_{1-x}\text{Rh}_x\text{Ge}$ compounds in fields applied along the c axis. Magnetization data of UCoGe are taken from Ref. [3] and URhGe from Ref. [29]. The arrows in (a) indicate T_C .

paramagnetic ground state. UTe_2 undergoes a sharp first-order metamagnetic transition (MT) at $H_m = 35$ T [21–23]. The superconducting phase is more pronounced on approaching H_m but is suddenly suppressed above H_m [24]. The relationship between the observed metamagnetic and superconducting transitions is presently the subject of intensive research.

Here, we focus on the field evolution of the ferromagnetic phase through the substituted $\text{UCo}_{1-x}\text{Rh}_x\text{Ge}$ system. To explore the anisotropic aspects, we have prepared single crystals of $\text{UCo}_{1-x}\text{Rh}_x\text{Ge}$ of several characteristic compositions and measured their magnetization (M) as a function of temperature (T) and magnetic field (H) applied along the b and c axis, respectively. The temperature dependences of specific heat (C_p) were also measured. T_C reaches the maximum value at $x = 0.4$. We have observed striking differences between the Co-rich ($x < 0.4$) and Rh-rich ($x > 0.4$) compounds with an abrupt change of the character of the ferromagnetic phase and the various paramagnetic regimes [10] in the T - x and H - x phase diagrams.

II. EXPERIMENT

We have grown substituted $\text{UCo}_{1-x}\text{Rh}_x\text{Ge}$ compounds with compositions $x = 0.1, 0.2, 0.3, 0.4$, and 0.8 in the form of single crystals by the Czochralski method in a tetra-arc furnace. Samples were thermally treated at 900°C [25,26] and the composition was tested by Electron-probe analyzer EPMA JXA-8900 (JEOL). Structural characterization by single-crystal x-ray diffraction using a Rigaku RAPID diffractometer evaluated using SHELX software [27] confirmed the orthorhombic TiNiSi -type structure—see the results summarized in the Appendix. The temperature and magnetic-field dependent magnetization M in static fields up to 7 T were measured using a commercial magnetometer MPMS 7T (Quantum Design). The specific-heat measurement was carried out down to 1.8 K using a homemade device in a top-loading Oxford cryostat. The high-field magnetization measurements in pulsed magnetic fields up to 57 T were performed using a nondestructive pulsed-field magnet, with a typical pulse duration of ~ 36 ms, installed at the International Mega Gauss Science Laboratory of the Institute for Solid State Physics at the University of Tokyo. The magnetization was measured

at 1.3 K by a conventional induction method with coaxial pickup coils using samples in the form of a bar having typical dimensions $0.75 \times 0.75 \times 2.5$ (b axis) mm^3 . The sample was immersed in super fluid He.

III. EXPERIMENTAL RESULTS

A. Low-field magnetization

The temperature dependence of magnetization of $\text{UCo}_{1-x}\text{Rh}_x\text{Ge}$ in a magnetic field of 0.01 T applied along the easy c direction is shown in Fig. 1(a). The T_C values of the studied compositions estimated as the temperatures of the maximum of the derivative $\partial M/\partial T$ [see arrows in Fig. 1(a)] values in Table I agree well with the reported values in Ref. [18]. T_C is equal to 2.5 K for UCoGe and increases steeply with substituting Co by Rh up to the maximum value of 20 K for $\text{UCo}_{0.6}\text{Rh}_{0.4}\text{Ge}$. Further increase of Rh concentration leads to a relatively slow decrease of T_C towards 9.5 K for the end member URhGe . The spontaneous magnetization (μ_s) simultaneously increases from $\mu_s = 0.05 \mu_B/\text{f.u.}$ (UCoGe) to the maximum of $0.50 \mu_B/\text{f.u.}$ ($\text{UCo}_{0.6}\text{Rh}_{0.4}\text{Ge}$) with increasing x (we notice here that the very weak μ_s of UCoGe is strongly sample dependent [3,28]) and then it decreases almost linearly to $\mu_s = 0.42 \mu_B/\text{f.u.}$ for URhGe [1] [Fig. 1(b)].

The temperature dependencies of magnetization for $H||b$ are considerably different from the easy-magnetization-direction behavior. They are characterized by a maximum at T_{max} as illustrated in Fig. 2 and listed in Table I. The qualitative character of the sharp-peak anomaly at $T_{\text{max}} = T_C$ known as typical for URhGe [3,14,15] is conserved between URhGe and $\text{UCo}_{0.6}\text{Rh}_{0.4}\text{Ge}$. $T_{\text{max}}(x)$ and $T_C(x)$ curves separate when lowering Rh concentration below $x = 0.4$ towards UCoGe exhibiting $T_{\text{max}} = 37.5$ K and $T_C = 2.5$ K.

B. High-field magnetization

A sharp metamagnetic jump at 12.5 T in URhGe occurs when the b -axis magnetization reaches the value of μ_s [14]. In contrast, there is not a corresponding metamagnetic jump at $M = \mu_s$ for UCoGe . Contrary to the behavior seen in URhGe , a broad and weak upturn around $\mu_0 H_m \approx 47.5$ T was observed

TABLE I. Magnetic parameters of $\text{UCo}_{1-x}\text{Rh}_x\text{Ge}$ compounds. The T_C , μ_s , T_{\max} , H_m , and H_R were taken from the experimental data. dM/dH represents the slopes of the magnetization isotherms below H_m or H_R ; data are also displayed as the inset in Fig. 3. The calculated values of H_b were obtained using the formula $\mu_s = (dM_b/dH)H_b$ taken from Ref. [14].

$\text{UCo}_{1-x}\text{Rh}_x\text{Ge}$	T_C (K)	$\mu_s(\mu_B/\text{f.u.})$	T_{\max} (K)	H_m (T)	H_R (T)	dM/dH	H_b [14] (T)
$x = 0.0$ [3]	2.5	0.07 [28]	37.5	47.5		0.007	10
$x = 0.1$	7.2	0.13	28	40.0		0.0093	13.9
$x = 0.2$	15.0	0.29	21	28.4		0.013	22.3
$x = 0.3$	18.6	0.42	21	27.0		0.0143	29.4
$x = 0.4$	20.0	0.50	$=T_C$		23.7	0.0188	26.6
$x = 0.8$	13.7	0.45	$=T_C$		14.3	0.028	16.1
$x = 0.9$ [30,31]	11.8		$=T_C$		13.4		
$x = 1.0$	9.5 [1]	0.42 [1]	$=T_C$ [3]		12.5 [8,9]	0.031	13.5

on the b -axis magnetization isotherm of UCoGe [3]. We measured the b -axis magnetization for all the $\text{UCo}_{1-x}\text{Rh}_x\text{Ge}$ compounds at 1.3 K in order to trace the evolution of the metamagnetic anomalies over the entire Co/Rh concentration range—see Fig. 3.

As illustrated by dashed lines in Fig. 3, the three representative points of the metamagnetic anomalies, namely, the onset M_{ins} , inflection $M_{\text{inf.}}$, and the end M_{end} , occur at the identical values of magnetization ($M_{\text{ins}} \approx 0.35 \mu_B/\text{f.u.}$, $M_{\text{inf.}} \approx 0.41 \mu_B/\text{f.u.}$, and $M_{\text{end}} \approx 0.52 \mu_B/\text{f.u.}$) for all the $\text{UCo}_{1-x}\text{Rh}_x\text{Ge}$ compounds. The initial slope of magnetization (dM/dH) at M_{ins} (see inset of Fig. 3), is, however, approximately five times larger ($\sim 31 \text{ m}\mu_B/T$) for URhGe than for UCoGe ($\sim 7 \text{ m}\mu_B/T$).

C. Specific heat

The ferromagnetic transition in the $\text{UCo}_{1-x}\text{Rh}_x\text{Ge}$ compounds is well detectable in specific-heat data as a λ -type anomaly located at T_C . The T_C values are in good agreement with the corresponding T_C values determined from magnetization data. Already at first glance the C_p/T vs T plots in Fig. 4 can be divided into two groups. The Co-rich compounds ($x < 0.4$) are characterized by a very small peak height, $\Delta C_p/T$, at T_C . The λ -type peak becomes suddenly much higher for $x \geq 0.4$. No other anomaly has been detected on the C_p/T vs T plots for any of the studied compounds.

We evaluated the magnetic specific heat as

$$C_{\text{mag}} = C_p - \gamma T - \beta T^3, \quad (1)$$

where γ is the Sommerfeld coefficient representing the electron specific heat $C_e = \gamma T$ and $C_{\text{ph}} = \beta T^3$ is the phonon specific heat expressed within a simplified Debye model which was previously used for UTGe compounds [14,33–35]. This approach was successful for compositions with low T_C ($\leq 15\text{K}$). In Fig. 5 we show two representative examples and display also the magnetic entropy calculated as

$$S_{\text{mag}} = \int_0^T \frac{C_{\text{mag}}}{T} dT. \quad (2)$$

In cases where T_C exceeds 15 K, we could not find a reasonable fit using this simple quadratic function. Instead, a general polynomial function with dominant quadratic term was used (see the Appendix). It is interesting to note that the low-temperature magnetic specific heat C_{mag}/T becomes finite for $x \geq 0.4$, which is further analyzed in the discussion.

IV. DISCUSSION

We have collected magnetic parameters from all the studied compounds and constructed the T - x and H - x phase diagrams in Fig. 6. The T - x diagram has two distinctly different parts. For $x < 0.4$ the $M(T)$ dependencies are characterized by a broad maximum at T_{\max} showing up well above T_C while a sharp peak appears at $T_C = T_{\max}$ on the URhGe side ($x \geq 0.4$). It is worth noting the ferromagnetic (FM) region with an intriguing coincidence $T_C = T_{\max}$. The region extends to the FM limit of the isoelectronic $\text{URh}_{1-x}\text{Ir}_x\text{Ge}$ system [35], indicating that this phenomenon is very robust. The T_{\max} is attributed to a crossover to the so-called correlated paramagnetic (CPM) regime [13,36]. Thus, the cooling of the compounds with $0 < x < 0.4$ consist of a PM-CPM crossover at T_{\max} followed by a CPM-FM phase transition at T_C . The crossover at T_{\max} was also clearly detected by NMR and assigned to a development of ferromagnetic spin fluctuations [37,38]. In contrast, cooling of the compounds with $0.4 \leq x < 1$, results in a direct PM-FM phase transition at T_C .

Metamagneticlike anomalies were detected at identical values of magnetization $M_{\text{inf.}} \approx 0.41 \mu_B/\text{f.u.}$, independent of composition. We also note that this feature is conserved in the isostructural ferromagnet URhSi at the b -axis moment polarization crossover [39] and the b -axis metamagnetic transition of isoelectronic antiferromagnet UIrGe [40]. The gradual reduction of the characteristic field of the metamagneticlike features at 47.5 T, for UCoGe , to 12.5 T, for URhGe is connected with the gradually increasing slope of magnetization dM/dH throughout the entire system (Fig. 6). The detected metamagnetic fields H_m vary with x in quite the same manner as the T_{\max} rather than T_C [Fig. 7(a)], in agreement with the proposed energy scale $1 \text{ K} \sim 1\text{T}$ [13] and confirmed by recent examples [22,35,40–42]. Thus, the energy scale for $x < 0.4$ is governed not by the ferromagnetic transition but by the mechanisms responsible for the metamagneticlike phenomena, similar to the behavior of URhSi [39]. The equality $T_C = T_{\max}$ between $\text{UCo}_{0.6}\text{Rh}_{0.4}\text{Ge}$ and URhGe results in scaling also with T_C [Fig. 7(a)].

The electrical resistivity behavior of UCoGe indicates the boundary of the ferromagnetic phase in the magnetic field along the b axis at $\sim 15 \text{ T}$ [11]—the blue point in the phase diagram in Fig. 6(b). Hardy *et al.* [14] have phenomenologically calculated the metamagnetic field for UCoGe along the b axis at $H_b \approx 12 \text{ T}$ using the relation $\mu_s = (dM_b/dH)H_b$,

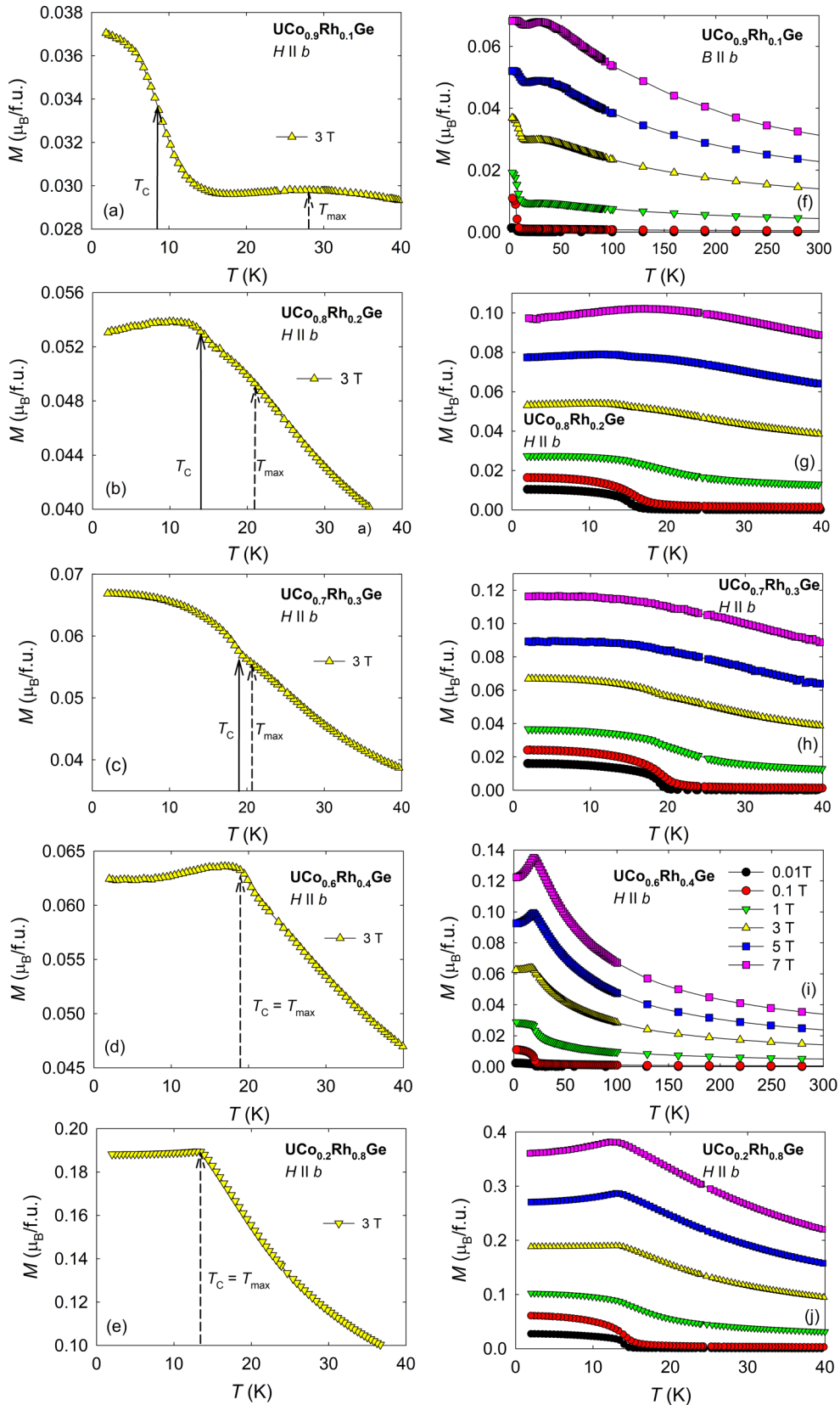


FIG. 2. Temperature dependencies of magnetization of $\text{UCo}_{1-x}\text{Rh}_x\text{Ge}$ compounds for several values of magnetic field applied along the b axis. Figures show the evolution of the T_C and T_{\max} throughout the $\text{UCo}_{1-x}\text{Rh}_x\text{Ge}$ system. Panels (a)–(e) show curves in a magnetic field of 3 T where the anomaly at T_{\max} is visible. The estimation of T_{\max} is difficult in $\text{UCo}_{0.7}\text{Rh}_{0.3}\text{Ge}$; T_{\max} seems to keep a similar value as $\text{UCo}_{0.8}\text{Rh}_{0.2}\text{Ge}$ but overlaid with the ferromagnetic signal due to an increasing T_C . Panels (f)–(j) show all recorded curves in various magnetic fields. Panels (f) and (i) representing $\text{UCo}_{0.6}\text{Rh}_{0.4}\text{Ge}$ and $\text{UCo}_{0.9}\text{Rh}_{0.1}\text{Ge}$ are displayed in full temperature scale as representative examples of $T_C = T_{\max}$ and $T_C < T_{\max}$ behavior.

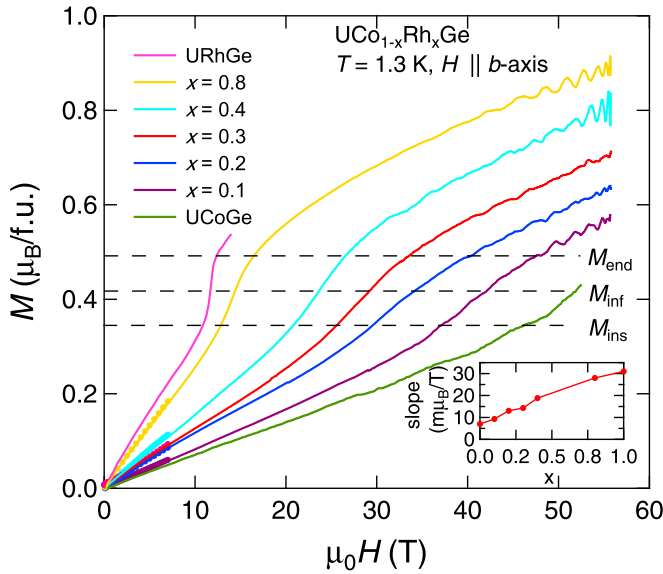


FIG. 3. Magnetization isotherms of all $\text{UCo}_{1-x}\text{Rh}_x\text{Ge}$ compounds measured in the b -axis pulsed field; data for parent compounds are identical to those reported in Ref. [3] and displayed with kind permission of authors W. Knafo and D. Aoki. The inset shows development of the magnetization slopes dM/dH at M_{ins} (see also Table I). The dashed lines indicate the onset M_{ins} , inflection M_{inf} , and the end M_{end} of the metamagnetic anomalies. The absolute values of the pulsed-field magnetization data were calibrated using precise superconducting quantum interference device magnetization data represented as dots in the magnetic field interval 0–7 T.

which seems to be in qualitative agreement with the experiment [11]. However, the b -axis magnetization curve of UCoGe has shown the upturn of magnetization exclusively at $\mu_0H_m = 47.5$ T [3] without any feature at 12 or 15 T. Similarly, no anomaly on the $M(H)$ curves in the field interval below H_m was detected in any other compounds with

$x < 0.4$. We have performed the identical analysis to Hardy *et al.* for all compounds and the results are summarized in Table I and plotted in Fig. 7(b). The calculated values of H_b gradually deviate from the experimentally determined H_m values for x decreasing from 0.4 to 0. We have tentatively drawn H_b with a dashed line in Fig. 6(b), as a FM \leftrightarrow CPM crossover.

We have also calculated the slope of magnetization along the easy magnetization axis (Fig. 8). The dependence is almost flat, $x \geq 0.4$, while it rapidly increases for x decreasing from 0.4 to 0. The large slope of $M(H)$ curves on the UCoGe side could also be the reason why the formula for H_b does not scale with H_m . The spontaneous magnetization becomes very different from the magnetization at high field due to enhanced ferromagnetic fluctuations in Co rich compounds.

The low-temperature FM-PPM (polarized paramagnet) first-order MT in URhGe at H_R is confirmed through the observations of the tricritical point [15] and a wing-type phase diagram [9]. Moreover, the MT in URhGe is accompanied by a Fermi-surface reconstruction [8]. In contrast to theoretical predictions for clean ferromagnets [44–46], the identical wing-type phase diagram was reported for $\text{UCo}_{0.1}\text{Rh}_{0.9}\text{Ge}$ by NMR [30,31]. Therefore, we suppose that this robust feature of field-induced FM-PPM transition is conserved in all $T_C = T_{\text{max}}$ $\text{UCo}_{1-x}\text{Rh}_x\text{Ge}$ compounds. On the other hand, taking into account the reported phase diagrams for UCoGe in Refs. [3,32], and our results, an increasing magnetic field along the b axis drives a FM $\xrightarrow{H_b}$ CPM $\xrightarrow{H_m}$ PPM sequence in all $T_C < T_{\text{max}}$ $\text{UCo}_{1-x}\text{Rh}_x\text{Ge}$ compounds. The FM-CPM boundary was not detected by pulsed-field magnetization, and in the UCoGe case, was suggested to be of rather crossoverlike character [11]. Accordingly, the invisibility of a FM $\xrightarrow{H_b}$ CPM crossover can signal an identical type of crossover in all $T_C < T_{\text{max}}$ $\text{UCo}_{1-x}\text{Rh}_x\text{Ge}$ compounds. It is worth mentioning that the H - T phase diagram of UCoGe is unique by missing a FM \rightarrow PPM MT, because the CPM completely surrounds the FM dome.

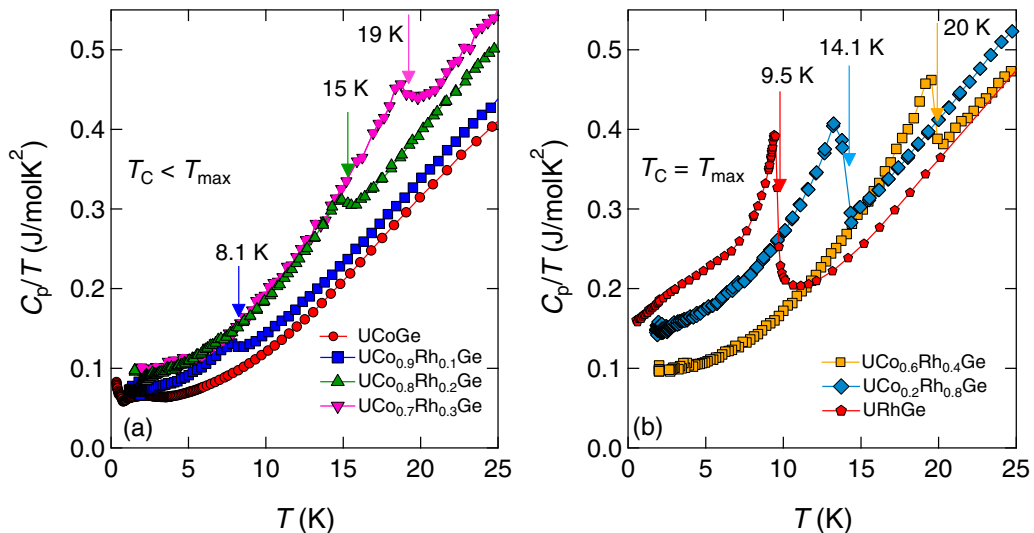


FIG. 4. The temperature dependence of specific heat (C_p/T vs T plots) of $\text{UCo}_{1-x}\text{Rh}_x\text{Ge}$ compounds for (a) $x < 0.4$ (with $T_C < T_{\text{max}}$) and (b) $x \geq 0.4$ (with $T_C = T_{\text{max}}$). The arrows indicate T_C . Data for the parent compounds UCoGe and URhGe have been taken from Refs. [26] and [32], respectively.

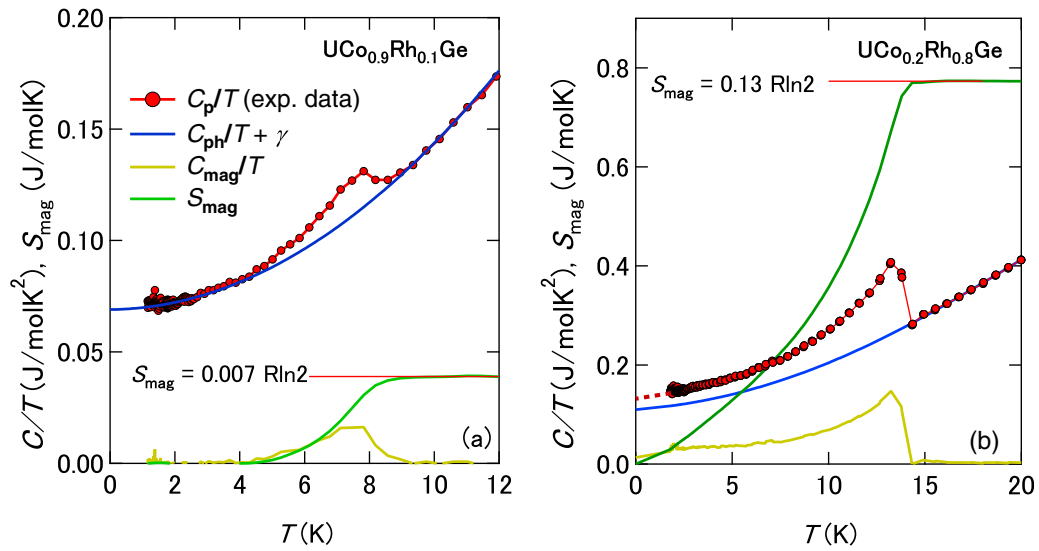


FIG. 5. The temperature dependence of specific heat and its components (C/T vs T plots) and magnetic entropy S_{mag} for (a) $x = 0.1$ and (b) $x = 0.8$. The value of S_{mag} is also expressed in the unit $R \ln 2$ at the red horizontal hairline.

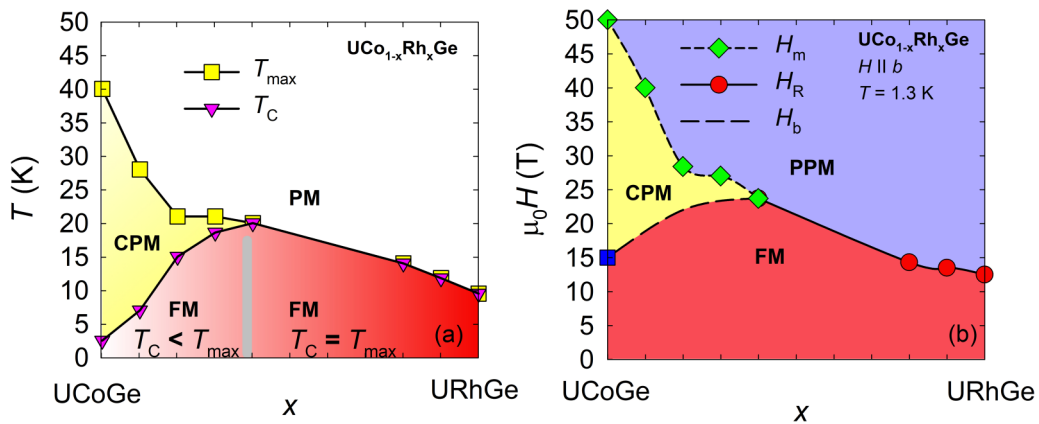


FIG. 6. (a) T - x and (b) H - x phase diagrams of the $\text{UCo}_{1-x}\text{Rh}_x\text{Ge}$ system. The value of T_{max} , H_R , and H_m for URhGe and UCoGe, respectively, were taken from Ref. [3]. The blue point in panel (b) marks the critical field of the ferromagnetic phase boundary in UCoGe; the point was taken from Ref. [11]. The long-dashed line in the H - x diagram tentatively indicates the evolution of $\text{FM} \rightarrow \text{CPM}$ crossover at H_b . The grey line in the T - x diagrams in panel (a) tentatively separates the low- and high- S_{mag} concentration regions.

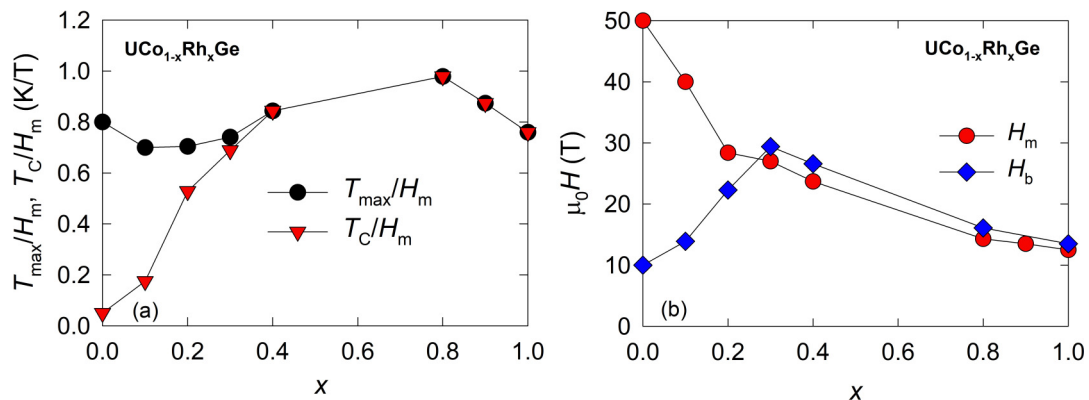


FIG. 7. (a) The concentration dependencies of (a) the T_{max}/H_m and T_C/H_m ratios and (b) the measured H_m and calculated H_b characteristic fields of metamagneticlike anomalies for $\text{UCo}_{1-x}\text{Rh}_x\text{Ge}$ compounds.

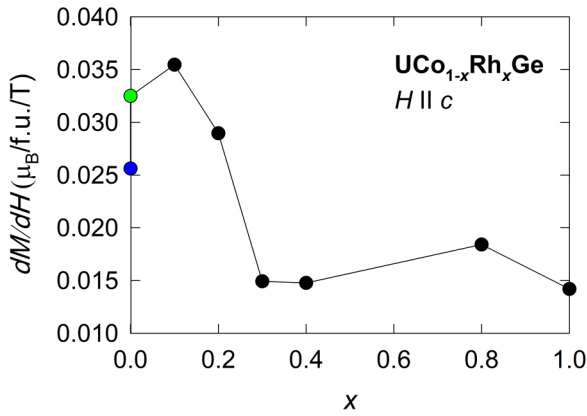


FIG. 8. The concentration dependence of the average slope of the magnetization curve in a field along the easy magnetization axis (c axis). The slope was calculated for the magnetic field interval 1–7 T. The point for URhGe was calculated from data in Ref. [29] and points for UCoGe from data in Ref. [3] [green point: pulsed-field data in Fig. 1(b)] and Ref. [43] (blue point: steady-field data in the interval 1–5 T). Two different values for UCoGe are caused by a strong sample dependence of FM parameters [25,26] but also different sweep rate of magnetic field.

Our detailed knowledge of the transitions and crossovers between PM, CPM, PPM, and FM allows us to explain the different shapes of the superconducting reentrant domes for both parent compounds. The FM $\xrightarrow{H_R}$ PPM MT of Lifshitz type in URhGe is connected with an increase of both the longitudinal and transversal magnetic fluctuations supporting the superconducting state [15]. However, this first-order MT to the PPM resulting in polarization of the magnetic moments towards the b axis must necessarily lead to a sudden freezing of the magnetic fluctuations. Therefore, the reentrant superconductivity sharply disappears above H_R . In contrast, the FM $\xrightarrow{H_b}$ CPM crossover in UCoGe does not polarize the magnetic moments. Therefore, it is not prohibitive for the spin fluctuations and the superconducting state can survive in the CPM to very high fields with the enormous $H_{c2(0)}$ [12] (and above p_c [47], where the CPM should exist as well). The field-induced transition from the FM state in UCoGe and URhGe is evidently of a different nature and apparently terminates in different paramagnetic states, the CPM and PPM of different Fermi surfaces, respectively.

Our scenario is in agreement with the observations in recently discovered paramagnetic heavy fermion superconductor UTe_2 [19,20]. UTe_2 shares qualitatively similar phenomena with ferromagnetic superconductors: a maximum in the magnetic susceptibility at $T_{\max} = 35$ K and a first-order MT at $\mu_0 H_m = 35$ T for $H \parallel b$ [21,22,39]. From this point of view the H - T phase diagram of UTe_2 consists of a CPM dome [22]. Superconductivity is preserved throughout the CPM regime in field along b and seems to be sharply delimited by the MT [24]. The field reinforcement of superconductivity near the critical field H_m is expected to be caused by magnetic fluctuations connected with Fermi-surface reconstruction [24] as well as the signature of a first-order MT is observed up to a critical end point at $T_{\text{CEP}} = 7$ K [22]. The relation between

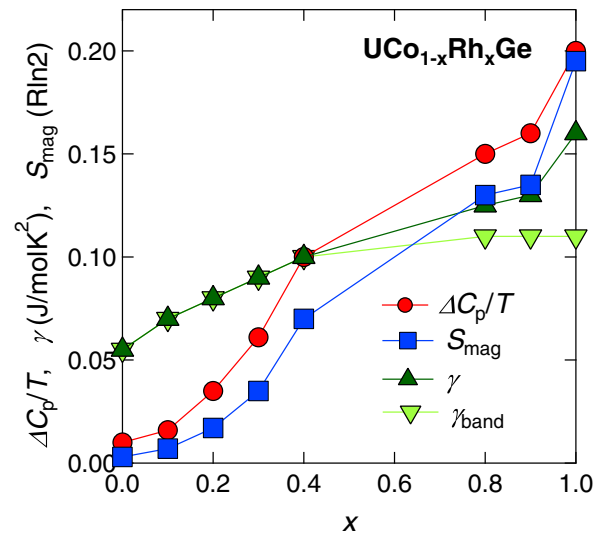


FIG. 9. The evolution of the parameters S_{mag} , γ , and height of peak $\Delta C_p/T$ at ferromagnetic transitions for all compositions in $\text{UCo}_{1-x}\text{Rh}_x\text{Ge}$.

metamagnetism and superconductivity in UTe_2 is the subject of continuing research [24].

The analysis of the specific-heat data is summarized in Fig. 9. We have plotted the evolution of the magnetic entropy S_{mag} , γ , and the height of the $\Delta C_p/T$ peak at the ferromagnetic transitions. The evolution of the parameters can be split at the first sight into two regions with respect to the presence of a CPM. The specific-heat data of compounds with $T_C < T_{\max}$ are characterized by a low height ($\Delta C_p/T$) of the λ -type anomaly and related low S_{mag} of the CPM $\xrightarrow{T_C}$ FM transition, while all compounds with $T_C = T_{\max}$ have significantly higher height ($\Delta C_p/T$) of the λ -type anomaly and related S_{mag} of the PM $\xrightarrow{T_C}$ FM transition. UCoGe is a model example of a weak itinerant ferromagnet [2,48,49]. The value of S_{mag} in itinerant ferromagnetic systems has been theoretically treated by Mohn [50] based on a Stoner model for the ideal itinerant system resulting in $S_{\text{mag}} = 0$. The rapid increase of S_{mag} in the UCoGe – $\text{UCo}_{0.6}\text{Rh}_{0.4}\text{Ge}$ region signals localization of the U moment. Regardless of the growth of S_{mag} towards URhGe, $S_{\text{mag}} = 0.2R\text{Ln}2$ is very low for the fully localized moment, however two orders of magnitude higher than that of UCoGe [2]. Low magnetic entropy on the UCoGe side may also suggest that a significant fraction of the entropy is not attributable to heavy quasiparticles but is instead carried by local moments which in UCoGe enter a more correlated state above T_C than in URhGe.

We paid extra attention to the γ coefficient evaluation. This subject was analyzed by Hardy and Miyake for URhGe and described by effective mass m^* ($\sim \gamma^*$) as a sum:

$$m^* = m^{\text{band}} + m^{**},$$

where m^{band} is the renormalized band mass, and m^{**} is the correlated mass associated with the magnetic instability [6,14]. The reentrant superconductivity was explained in URhGe by the mass enhancement though the correlation term γ^{**} when approaching H_R [6]. Our specific-heat data analysis, within this scope, revealed $\gamma^* = \gamma^{\text{band}}$ for all compounds with

$T_C < T_{\max}$. For all compositions with $T_C = T_{\max}$, however, we found $\gamma^* > \gamma^{\text{band}}$. The γ^* grows towards URhGe through the correlation term γ^{**} (Fig. 9). Applying the magnetic field along the b axis, m^{**} increases further on approaching H_R , and thus the superconducting phase reemerges near H_R . A similar trend is also observed in UTe_2 [21,22,51].

V. CONCLUSIONS

We have successfully studied magnetic phenomena for a magnetic field applied along the b axis throughout the $\text{UCo}_{1-x}\text{Rh}_x\text{Ge}$ system by investigation of a large series of single crystals and have constructed unique T - x and H - x diagrams. The characteristic temperature T_{\max} , where magnetization shows a maximum, splits the phase diagram to two parts: The $\text{UCoGe} - \text{UCo}_{0.6}\text{Rh}_{0.4}\text{Ge}$ region with $T_C < T_{\max}$, and the $\text{UCo}_{0.6}\text{Rh}_{0.4}\text{Ge} - \text{URhGe}$ region with $T_C = T_{\max}$. We have detected metamagnetic anomalies at H_m which correlate with the value of T_{\max} by a $1 \text{ K} \approx 1 \text{ T}$ scale. Based on these findings we have drawn three distinct paramagnetic regions in the phase diagram: paramagnet, PM; correlated paramagnet, CPM; and polarized paramagnet, PPM. The CPM exists only in the part of the phase diagram with $T_C < T_{\max}$ and overlays the ferromagnetic phase. It has consequences in the low-temperature magnetization processes: a $\text{FM} \xrightarrow{H_b} \text{CPM} \xrightarrow{H_m} \text{PPM}$ sequence was found with increasing magnetic field within the $T_C < T_{\max}$ region; while a direct $\text{FM} \xrightarrow{H_R} \text{PPM}$ transition is detected for compositions within $T_C = T_{\max}$. The pulsed-field magnetization study has not detected any sign of the $\text{FM} \xrightarrow{H_b} \text{CPM}$ magnetization anomaly, even though the T_C and spontaneous magnetic moments μ_s are significantly enhanced in the alloy compounds in contrast to the very low values for the parent UCoGe . Values of H_b were calculated from our experimental data in agreement with the value found by electrical resistivity for UCoGe . We conclude that the simple model of metamagnetism at H_R in URhGe , as well as for all $T_C = T_{\max}$ compounds, is not applicable to UCoGe and all $T_C < T_{\max}$ compounds characterized by two critical fields H_b and H_m . It is also important to note that the metamagnetic-like transition takes place when the magnetization along the b axis reaches a critical value of $M_{\text{inf}} \approx 0.41 \mu_B/\text{f.u.}$, which is independent of composition. The nature of the crossovers at H_m and particularly H_b is the subject of further research, in contrast to the well-established first-order MT at H_R .

The ferromagnetic transition $\text{CPM} \xrightarrow{T_C} \text{FM}$ for $T_C < T_{\max}$ compounds is characterized by a very low magnetic entropy

S_{mag} , which is in contrast to the suddenly higher S_{mag} for compositions where the CPM is missing. Nonmonotonous evolution of S_{mag} may signal a sudden localization of the U magnetic moment for compositions with $T_C = T_{\max}$. To verify the scenario of delocalization of the magnetic moments towards UCoGe or their potential correlations connected with the ferromagnetic spin fluctuations in CPM, a magnetic neutron-scattering investigation is highly desirable. The $\text{FM} \xrightarrow{H_b} \text{CPM}$ crossover in UCoGe explains well the extremely high $H_{c2(0)}$ of the superconducting state along the b axis, in contrast to the sharp superconducting dome in URhGe where a first-order $\text{FM} \xrightarrow{H_R} \text{PPM}$ MT results in polarization of the magnetic moments.

ACKNOWLEDGMENTS

This work was supported by JSPS KAKENHI Grants No. JP15H05884 (J-Physics), No. JP20K03854, and No. JP16K05463. This project was supported by OP VVV project MATFUN under Grant No. CZ.02.1.01/0.0/0.0/15_003/0000487. The authors would like to thank D. Aoki and W. Knafo for providing the magnetization isotherms of pure URhGe and UCoGe and discussion of our data. We are indebted to R. H. Colman for making language corrections. The experiments were performed at MGML [52], which was supported within the program of Czech Research Infrastructures (Project No. LM2018096).

APPENDIX

The Appendix chapter extends the chapter Experimental results about additional data, which are useful for understanding of the complex magnetic phase diagram of $\text{UCo}_{1-x}\text{Rh}_x\text{Ge}$ compounds. Tables II–VIII summarize evaluated crystal structure parameters for each studied compound. Panels in Fig. 10 show low temperature magnetization isotherms along all three crystallographic directions to support our conclusions about the magnetocrystalline anisotropy of the $\text{UCo}_{1-x}\text{Rh}_x\text{Ge}$ compounds. Figure 11 is the extension of the Fig. 5 to show specific heat data for all compounds and support the constructed evolutions of thermodynamic parameters in Fig. 9. Figure 12 graphically shows the selected data from Tables II–VIII to support the Vegard-law behavior of the lattice parameters of the compounds in the $\text{UCo}_{1-x}\text{Rh}_x\text{Ge}$ system.

TABLE II. Crystal structure parameters of UCoGe .

		a (Å)	b (Å)	c (Å)	V (Å) ³	$d_{\text{U-U}}$ (Å)	
UCoGe		6.8533(5)	4.2098(3)	7.2374(5)	208.814	3.4808(4)	
Atom	x/a	y/b	z/c	Occ.	U	Site	Sym.
U	0.009 98(11)	0.25	0.707 82(12)	1	0.006	4c	.m.
Ge	0.1971(3)	0.25	0.0866(3)	1	0.006	4c	.m.
Co	0.2883(5)	0.25	0.4173(4)	1	0.009	4c	.m.

TABLE III. Crystal structure parameters of $\text{UCo}_{0.9}\text{Rh}_{0.1}\text{Ge}$.

		a (Å)	b (Å)	c (Å)	V (Å) ³	$d_{\text{U-U}}$ (Å)	
$\text{UCo}_{0.9}\text{Rh}_{0.1}\text{Ge}$		6.8484(3)	4.2153(2)	7.2594(4)	209.565	3.4869(6)	
Atom	x/a	y/b	z/c	Occ.	U	Site	Sym.
U	0.009 99(15)	0.25	0.791 52(19)	1	0.006	4c	.m.
Ge	0.1969(5)	0.25	0.4137(5)	1	0.006	4c	.m.
Co	0.2887(7)	0.25	0.0822(6)	0.92(4)	0.009	4c	.m.
Rh	0.2887(7)	0.25	0.0822(6)	0.08(4)	0.009	4c	.m.

TABLE IV. Crystal structure parameters of $\text{UCo}_{0.8}\text{Rh}_{0.2}\text{Ge}$.

		a (Å)	b (Å)	c (Å)	V (Å) ³	$d_{\text{U-U}}$ (Å)	
$\text{UCo}_{0.8}\text{Rh}_{0.2}\text{Ge}$		6.8583(3)	4.2310(2)	7.2973(3)	211.749	3.4871(3)	
Atom	x/a	y/b	z/c	Occ.	U	Site	Sym.
U	0.009 57(6)	0.25	0.793 36(7)	1	0.005	4c	.m.
Ge	0.1960(2)	0.25	0.4131(2)	1	0.007	4c	.m.
Co	0.2880(3)	0.25	0.0826(3)	0.781(18)	0.009	4c	.m.
Rh	0.2880(3)	0.25	0.0826(3)	0.219(18)	0.009	4c	.m.

TABLE V. Crystal structure parameters of $\text{UCo}_{0.7}\text{Rh}_{0.3}\text{Ge}$.

		a (Å)	b (Å)	c (Å)	V (Å) ³	$d_{\text{U-U}}$ (Å)	
$\text{UCo}_{0.7}\text{Rh}_{0.3}\text{Ge}$		6.8643(5)	4.2480(3)	7.3333(6)	213.838	3.4994(4)	
Atom	x/a	y/b	z/c	Occ.	U	Site	Sym.
U	0.009 47(8)	0.25	0.793 62(12)	1	0.007	4c	.m.
Ge	0.1954(3)	0.25	0.4137(3)	1	0.009	4c	.m.
Co	0.2879(3)	0.25	0.0825(3)	0.68(2)	0.010	4c	.m.
Rh	0.2879(3)	0.25	0.0825(3)	0.32(2)	0.010	4c	.m.

TABLE VI. Crystal structure parameters of $\text{UCo}_{0.6}\text{Rh}_{0.4}\text{Ge}$.

		a (Å)	b (Å)	c (Å)	V (Å) ³	$d_{\text{U-U}}$ (Å)	
$\text{UCo}_{0.6}\text{Rh}_{0.4}\text{Ge}$		6.8640(2)	4.2563(1)	7.3601(3)	215.027	3.4918(4)	
Atom	x/a	y/b	z/c	Occ.	U	Site	Sym.
U	0.009 20(12)	0.25	0.793 70	1	0.003	4c	.m.
Ge	0.1949(4)	0.25	0.41360	1	0.005	4c	.m.
Co	0.2880(4)	0.25	0.083 50	0.46(4)	0.007	4c	.m.
Rh	0.2880(4)	0.25	0.083 50	0.54(4)	0.007	4c	.m.

TABLE VII. Crystal structure parameters of $\text{UCo}_{0.2}\text{Rh}_{0.8}\text{Ge}$.

		a (Å)	b (Å)	c (Å)	V (Å) ³	$d_{\text{U-U}}$ (Å)	
$\text{UCo}_{0.2}\text{Rh}_{0.8}\text{Ge}$		6.8766(3)	4.3063(2)	7.4646(3)	221.047	3.5044(3)	
Atom	x/a	y/b	z/c	Occ.	U	Site	Sym.
U	0.008 52(5)	0.25	0.795 38(6)	1	0.006	4c	.m.
Ge	0.193 40(18)	0.25	0.412 98(17)	1	0.008	4c	.m.
Co	0.287 55(15)	0.25	0.084 27(14)	0.159(10)	0.008	4c	.m.
Rh	0.287 55(15)	0.25	0.084 27(14)	0.841(10)	0.007	4c	.m.

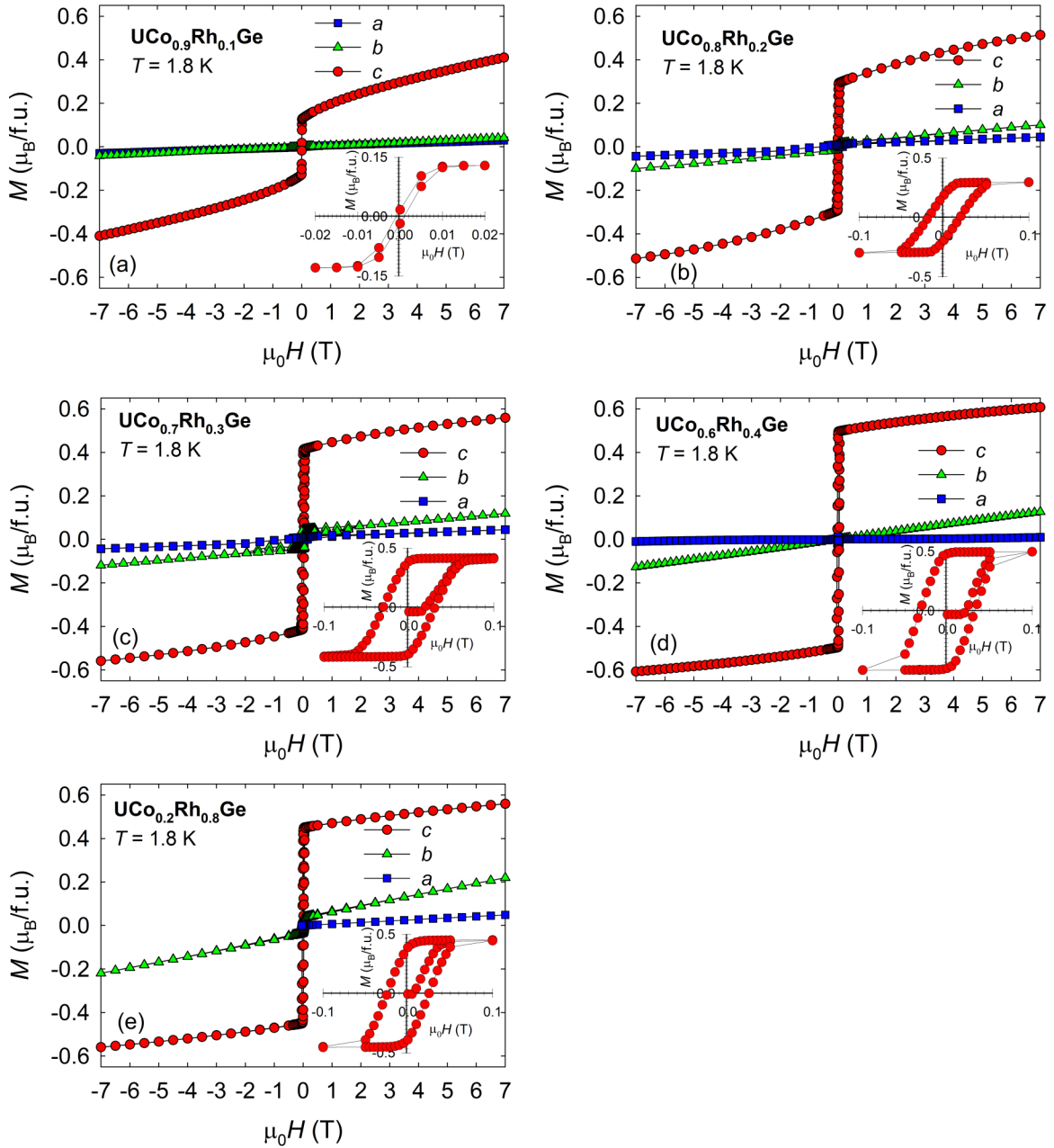


FIG. 10. The magnetization loops along all three crystallographic axes of all alloy compounds in the $\text{UCo}_{1-x}\text{Rh}_x\text{Ge}$ system for $x = 0.1$ (a), 0.2 (b), 0.3 (c), 0.4 (d), and 0.8 (f). Panels are displayed in the identical magnetization scale to enhance the evolution of spontaneous (μ_s) and saturated magnetizations.

TABLE VIII. Crystal structure parameters of URhGe.

		a (Å)	b (Å)	c (Å)	V (Å) ³	$d_{\text{U-U}}$ (Å)	
URhGe		6.8902(11)	4.3326(7)	7.5184(14)	224.34	3.5139(5)	
Atom	x/a	y/b	z/c	Occ.	U	Site	Sym.
U	0.008 18(6)	0.25	0.703 98(6)	1	0.006	4c	.m.
Ge	0.1928(2)	0.25	0.086 95(18)	1	0.008	4c	.m.
Rh	0.287 62(16)	0.25	0.415 60(13)	1	0.006	4c	.m.

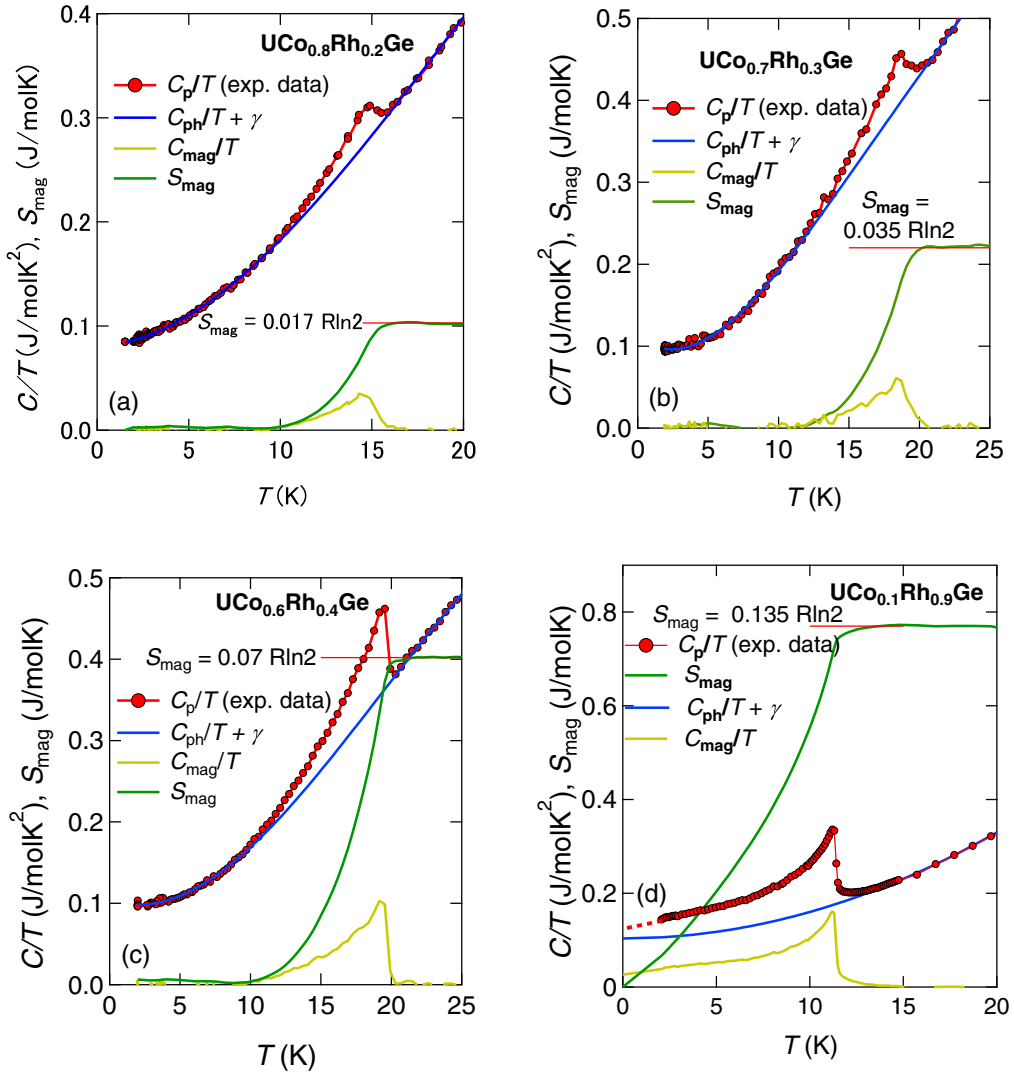


FIG. 11. Specific-heat data of all compounds in $\text{UCo}_{1-x}\text{Rh}_x\text{Ge}$ system with the evaluated values of magnetic entropy S_{mag} for $x = 0.2$ (a), 0.3 (b), 0.4 (c), and 0.9 (d). The value of S_{mag} is also displayed in the $R \ln 2$ scale and marked by the red horizontal hairline. A general polynomial function with dominant quadratic term was used for composition with $T_C > 15$ K where the simple Debye $\sim T^2$ dependence does not provide usable result to extract the phonon contribution.

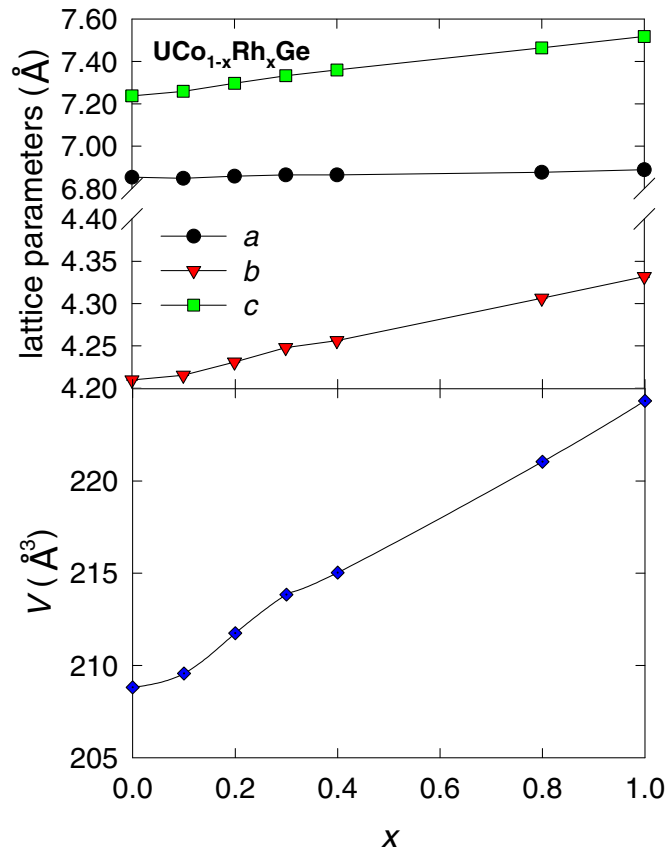


FIG. 12. Lattice parameters throughout the $\text{UCo}_{1-x}\text{Rh}_x\text{Ge}$ system; error bars are smaller than the size of points.

- [1] D. Aoki, A. Huxley, E. Ressouche, D. Braithwaite, J. Flouquet, J. P. Brison, E. Lhotel, and C. Paulsen, *Nature (London)* **413**, 613 (2001).
- [2] N. T. Huy, A. Gasparini, D. E. de Nijs, Y. Huang, J. C. P. Klaasse, T. Gortenmulder, A. de Visser, A. Hamann, T. Gorch, and H. von Löhneysen, *Phys. Rev. Lett.* **99**, 067006 (2007).
- [3] W. Knafo, T. D. Matsuda, D. Aoki, F. Hardy, G. W. Scheerer, G. Ballon, M. Nardone, A. Zitouni, C. Meingast, and J. Flouquet, *Phys. Rev. B* **86**, 184416 (2012).
- [4] F. Levy, I. Sheikin, B. Grenier, and A. D. Huxley, *Science* **309**, 1343 (2005).
- [5] A. Miyake, D. Aoki, and J. Flouquet, *J. Phys. Soc. Jpn.* **78**, 063703 (2009).
- [6] A. Miyake, D. Aoki, and J. Flouquet, *J. Phys. Soc. Jpn.* **77**, 094709 (2008).
- [7] D. Aoki, G. Knebel, and J. Flouquet, *J. Phys. Soc. Jpn.* **83**, 094719 (2014).
- [8] A. Gourgout, A. Pourret, G. Knebel, D. Aoki, G. Seyfarth, and J. Flouquet, *Phys. Rev. Lett.* **117**, 046401 (2016).
- [9] S. Nakamura, T. Sakakibara, Y. Shimizu, S. Kittaka, Y. Kono, Y. Haga, J. Pospíšil, and E. Yamamoto, *Phys. Rev. B* **96**, 094411 (2017).
- [10] J. Pospíšil, Y. Haga, A. Miyake, S. Kambe, N. Tateiwa, Y. Tokunaga, F. Honda, A. Nakamura, Y. Homma, M. Tokunaga, D. Aoki, and E. Yamamoto, *Physica B: Condens. Matter* **536**, 532 (2018).
- [11] D. Aoki, T. D. Matsuda, V. Taufour, E. Hassinger, G. Knebel, and J. Flouquet, *J. Phys. Soc. Jpn.* **78**, 113709 (2009).
- [12] B. L. Wu, G. Bastien, M. Taupin, C. Paulsen, L. Howald, D. Aoki, and J. P. Brison, *Nat. Commun.* **8**, 14480 (2017).
- [13] D. Aoki, W. Knafo, and I. Sheikin, *C. R. Phys.* **14**, 53 (2013).
- [14] F. Hardy, D. Aoki, C. Meingast, P. Schweiss, P. Burger, H. Von Löhneysen, and J. Flouquet, *Phys. Rev. B* **83**, 195107 (2011).
- [15] D. Braithwaite, D. Aoki, J. P. Brison, J. Flouquet, G. Knebel, A. Nakamura, and A. Pourret, *Phys. Rev. Lett.* **120**, 037001 (2018).
- [16] G. Bastien, A. Gourgout, D. Aoki, A. Pourret, I. Sheikin, G. Seyfarth, J. Flouquet, and G. Knebel, *Phys. Rev. Lett.* **117**, 206401 (2016).
- [17] G. Bastien, D. Braithwaite, D. Aoki, G. Knebel, and J. Flouquet, *Phys. Rev. B* **94**, 125110 (2016).
- [18] N. T. Huy and A. de Visser, *Solid State Commun.* **149**, 703 (2009).
- [19] S. Ran, C. Eckberg, Q. P. Ding, Y. Furukawa, T. Metz, S. R. Saha, I. L. Liu, M. Zic, H. Kim, J. Paglione, and N. P. Butch, *Science* **365**, 684 (2019).

- [20] D. Aoki, A. Nakamura, F. Honda, D. X. Li, Y. Homma, Y. Shimizu, Y. J. Sato, G. Knebel, J. P. Brison, A. Pourret, D. Braithwaite, G. Lapertot, Q. Niu, M. Valiska, H. Harima, and J. Flouquet, *J. Phys. Soc. Jpn.* **88**, 043702 (2019).
- [21] A. Miyake, Y. Shimizu, Y. J. Sato, D. Li, A. Nakamura, Y. Homma, F. Honda, J. Flouquet, M. Tokunaga, and D. Aoki, *J. Phys. Soc. Jpn.* **88**, 063706 (2019).
- [22] W. Knafo, M. Valiska, D. Braithwaite, G. Lapertot, G. Knebel, A. Pourret, J. P. Brison, J. Flouquet, and D. Aoki, *J. Phys. Soc. Jpn.* **88**, 063705 (2019).
- [23] S. Ran, I. L. Liu, Y. S. Eo, D. J. Campbell, P. M. Neves, W. T. Fuhrman, S. R. Saha, C. Eckberg, H. Kim, D. Graf, F. Balakirev, J. Singleton, J. Paglione, and N. P. Butch, *Nat. Phys.* **15**, 1250 (2019).
- [24] G. Knebel, W. Knafo, A. Pourret, Q. Niu, M. Valiska, D. Braithwaite, G. Lapertot, M. Nardone, A. Zitouni, S. Mishra, I. Sheikin, G. Seyfarth, J. P. Brison, D. Aoki, and J. Flouquet, *J. Phys. Soc. Jpn.* **88**, 063707 (2019).
- [25] N. T. Huy, Y. K. Huang, and A. de Visser, *J. Magn. Magn. Mater.* **321**, 2691 (2009).
- [26] J. Pospíšil, K. Prokeš, M. Reehuis, M. Tovar, J. P. Vejpravová, J. Prokleška, and V. Sechovský, *J. Phys. Soc. Jpn.* **80**, 084709 (2011).
- [27] G. M. Sheldrick, *Acta Crystallogr. Sect. A* **64**, 112 (2008).
- [28] N. T. Huy, D. E. de Nijs, Y. K. Huang, and A. de Visser, *Phys. Rev. Lett.* **100**, 077002 (2008).
- [29] D. Aoki and J. Flouquet, *J. Phys. Soc. Jpn.* **81**, 011003 (2012).
- [30] Y. Tokunaga, D. Aoki, H. Mayaffre, S. Kramer, M. H. Julien, C. Berthier, M. Horvatic, H. Sakai, T. Hattori, S. Kambe, and S. Araki, *Phys. Rev. B* **93**, 201112(R) (2016).
- [31] Y. Tokunaga, D. Aoki, H. Mayaffre, S. Kramer, M. H. Julien, C. Berthier, M. Horvatic, H. Sakai, S. Kambe, and S. Araki, *Phys. Rev. Lett.* **114**, 216401 (2015).
- [32] D. Aoki, F. Hardy, A. Miyake, V. Taufour, T. D. Matsuda, and J. Flouquet, *C. R. Phys.* **12**, 573 (2011).
- [33] K. Prokes, T. Tahara, Y. Echizen, T. Takabatake, T. Fujita, I. H. Hagmusa, J. C. P. Klaasse, E. Brück, F. R. de Boer, M. Divis, and V. Sechovsky, *Physica B: Condens. Matter* **311**, 220 (2002).
- [34] K. Prokeš, T. Tahara, T. Fujita, H. Goshima, T. Takabatake, M. Mihalik, A. A. Menovsky, S. Fukuda, and J. Sakurai, *Phys. Rev. B* **60**, 9532 (1999).
- [35] J. Pospíšil, Y. Haga, S. Kambe, Y. Tokunaga, N. Tateiwa, D. Aoki, F. Honda, A. Nakamura, Y. Homma, E. Yamamoto, and T. Yamamura, *Phys. Rev. B* **95**, 155138 (2017).
- [36] W. Knafo, R. Settai, D. Braithwaite, S. Kurahashi, D. Aoki, and J. Flouquet, *Phys. Rev. B* **95**, 014411 (2017).
- [37] Y. Ihara, T. Hattori, K. Ishida, Y. Nakai, E. Osaki, K. Deguchi, N. K. Sato, and I. Satoh, *Phys. Rev. Lett.* **105**, 206403 (2010).
- [38] T. Hattori, Y. Ihara, Y. Nakai, K. Ishida, Y. Tada, S. Fujimoto, N. Kawakami, E. Osaki, K. Deguchi, N. K. Sato, and I. Satoh, *Phys. Rev. Lett.* **108**, 066403 (2012).
- [39] W. Knafo, T. D. Matsuda, F. Hardy, D. Aoki, and J. Flouquet, *Phys. Rev. B* **100**, 094421 (2019).
- [40] J. Pospíšil, Y. Haga, Y. Kohama, A. Miyake, S. Kambe, N. Tateiwa, M. Vališka, P. Proschek, J. Prokleška, V. Sechovsky, M. Tokunaga, K. Kindo, A. Matsuo, and E. Yamamoto, *Phys. Rev. B* **98**, 014430 (2018).
- [41] N. Tateiwa, S. Ikeda, Y. Haga, T. D. Matsuda, E. Yamamoto, K. Sugiyama, M. Hagiwara, K. Kindo, and Y. Onuki, *J. Phys. Soc. Jpn.* **80**, 014706 (2011).
- [42] Y. Hirose, T. Takeuchi, F. Honda, S. Yoshiuchi, M. Hagiwara, E. Yamamoto, Y. Haga, R. Settai, and Y. Onuki, *J. Phys. Soc. Jpn.* **84**, 074704 (2015).
- [43] K. Prokes, A. de Visser, Y. K. Huang, B. Fak, and E. Ressouche, *Phys. Rev. B* **81**, 180407(R) (2010).
- [44] M. Brando, D. Belitz, F. M. Grosche, and T. R. Kirkpatrick, *Rev. Mod. Phys.* **88**, 025006 (2016).
- [45] T. R. Kirkpatrick and D. Belitz, *Phys. Rev. B* **91**, 214407 (2015).
- [46] Y. Sang, D. Belitz, and T. R. Kirkpatrick, *Phys. Rev. Lett.* **113**, 207201 (2014).
- [47] E. Slooten, T. Naka, A. Gasparini, Y. K. Huang, and A. de Visser, *Phys. Rev. Lett.* **103**, 097003 (2009).
- [48] M. Vališka, J. Pospíšil, A. Stunault, Y. Takeda, B. Gillon, Y. Haga, K. Prokeš, M. M. Abd-Elmeguid, G. Nenert, T. Okane, H. Yamagami, L. Chapon, A. Gukasov, A. Cousson, E. Yamamoto, and V. Sechovský, *J. Phys. Soc. Jpn.* **84**, 084707 (2015).
- [49] M. Taupin, J.-P. Sanchez, J. P. Brison, D. Aoki, G. Lapertot, F. Wilhelm, and A. Rogalev, *Phys. Rev. B* **92**, 035124 (2015).
- [50] P. Mohn and G. Hilscher, *Phys. Rev. B* **40**, 9126 (1989).
- [51] S. Imajo, Y. Kohama, A. Miyake, C. Dong, M. Tokunaga, J. Flouquet, K. Kindo, and D. Aoki, *J. Phys. Soc. Jpn.* **88**, 083705 (2019).
- [52] <http://mgml.eu>.